Hydrodynamic Optimization Testing of Ballast-Free Ship Design

(NOTE: Please consult the 2008 report with additional data, available at www.glmri.org)

Final

Michael G. Parsons — Arthur F. Thurnau Professor
Professor of Naval Architecture and Marine Engineering
Phone: 734-763-3081; FAX: 734-936-882; e-mail: parsons@umich.edu

Miltiadis Kotinis — Assistant Professor, SUNY Maritime College
Phone: 734-709-6425; FAX: 516-767-1063; e-mail: mkotinis@umich.edu

October 30, 2007

Department of Naval Architecture and Marine Engineering
University of Michigan
2600 Draper Road
Ann Arbor, MI 48109-2145

Research funded in part by the Great Lakes Maritime Research Institute.
This study was supported by the U.S. Maritime Administration
Grant # DTMA1-G-06-005

Table of Contents

List of Tables

page

List of Figures

Executive Summary

The initial investigation of the Ballast-Free Ship concept demonstrated the feasibility of the concept though a thorough examination of various design aspects. The effectiveness of the concept, in terms of eliminating the transport of foreign ballast water from ships operating in the ballast condition, was also demonstrated by utilizing Computational Fluid Dynamics (CFD) software to simulate the flow in the double bottom ballast trunks of the vessel. Nevertheless, this initial investigation did not succeed in showing the full cost-effectiveness of the concept. The main reason was a significant fuel penalty that resulted from an increased power requirement found in the initial hydrodynamic testing of a non-optimized discharge configuration on an existing, higher-speed vessel with a non-optimum propeller.

The current phase of this research project focuses on the further hydrodynamic investigation of the Ballast-Free Ship concept; both experimental and numerical. The experimental investigation was performed by utilizing the Seaway-size bulk carrier model that was designed and built as part of the initial phase of this project; also sponsored by the GLMRI. The resistance and propulsion tests were performed in the towing tank of the University of Michigan Marine Hydrodynamic Laboratory in January 2007. The numerical investigation was performed utilizing commercial CFD software, namely FLUENT®.

The computational results were utilized both as guidance for the experimental setup and also to corroborate the experimental results. Specifically, the selection of the trunk flow inlet and outlet locations utilized in the towing tank experiments was guided by the numerical results. The ballast trunk flow inlet was located in the center of the bulbous bow. Two different locations were tested for the water discharge: one at the level of the upper part of the propeller disk close to Station 17 (near the forward engine room bulkhead, full scale) and one lower close to Station 19 (near the aft engine room bulkhead).

The experiments in the towing tank consisted of detailed resistance and propulsion testing with and without the ballast trunk flow. The analysis of the model test data revealed that the experimental results were in good agreement with the numerical results. Overall, discharging water at the stern of the model slightly increases ship resistance, but proper design of the discharging arrangements can overcome this negative effect. Another source of modest ship resistance increase is the trunk inlet at the bow. Given the limited positive-pressure region at the bow of the vessel, an inlet location other than that currently utilized will probably result in a significant reduction in the available pressure differential, without providing a noteworthy benefit in terms of ship resistance.

Nonetheless, the proper water discharge at the stern of the vessel has a favorable effect on the propulsion characteristics for the Seaway-size bulk carrier design investigated. The computed reduction in powering requirements, relative to the initial unmodified design, at an assumed ballast speed of 15.5 knots was 7.3% for water discharge close to Station 17 and 2.1% for water discharge close to Station 19. This gain in propulsive efficiency outweighs the increase in ship resistance. The method utilized for computing the ship propulsive requirement is based on a well-established extrapolation procedure that contains significant levels of uncertainty; therefore, only a full-scale implementation of the concept can provide a precise determination of the actual propulsive gains.

In order to investigate the economic benefit of the aforementioned propulsive improvements, a pragmatic operating scenario for the grain trade to Europe was adopted for the Ballast-Free bulk carrier. The change in the Required Freight Rate (RFR) with respect to an alternative filtration and UV ballast treatment system was calculated. The net savings would be $0.93 per ton of cargo for the water discharge close to Station 17 and $0.44 per ton of cargo for the water discharge close to Station 19. The overall ship design would also benefit from placement of the water discharge near the forward engine room bulkhead. A different operating scenario could result in even lower savings. Nevertheless, cost-effectiveness combined with a numerically-demonstrated foreign-ballast-elimination capability confirms the Ballast-Free Ship concept as a viable alternative to more costly ballast treatment systems. Even though the current project focuses on a smaller Seaway-size bulk carrier, the concept should also be applicable to other new-construction ships of different types and sizes.

1. Introduction

The Ballast-Free Ship Concept was invented (US Patent #6,694,908 2004) and initially investigated (Kotinis et al. 2004, Kotinis 2005, *Ballast Water News* 2004) at the University of Michigan as a way to minimize the risk of the further introduction of nonindigenous aquatic species into the Great Lakes and other coastal waters by ships arriving in the ballast condition. Even though the feasibility of the concept was demonstrated, the initial analysis was limited by its required comprehensive research scope and limited associated budget. Thus, it was only feasible to support model testing that utilized an existing model. Although the vessel type of greatest interest for the Great Lakes nonindigenous aquatic species introduction problem is the Seaway-sized bulk carrier, the best available model was of a relatively finer, higher-speed barge-carrying Lighter Aboard Ship (LASH) vessel. This existing model was modified to utilize a more conventional stern, but the model test results were not directly applicable to the Seaway-sized bulk carriers studied in detail in the rest of the research effort.

The first year of GLMRI sponsored research (Parsons and Kotinis 2006) supported the design of a typical Seaway-sized bulk carrier and the construction of a scaled model to be utilized in subsequent towing tank experiments. This model was designed, constructed, and delivered in 2006. The goal was to use this model to optimize the location of the Ballast-Free trunk discharges in order to reduce or eliminate the propulsion power increase observed with the modified LASH model. The experimental and numerical hydrodynamic investigation, combined with an optimization procedure, was expected to lead to a design solution that could offer a net savings in Required Freight Rate (RFR) relative to alternate ballast water treatment methods and approaches.

In the present research, the hydrodynamic aspects of the Ballast-Free Ship concept were further investigated both experimentally and numerically. The initial results of the experimental program were reported in the popular press in January (Parsons 2007). Part of the numerical investigation, including an attempt at discharge location design optimization, was reported in a paper presented at the 9th International Conference on Numerical Ship Hydrodynamics (Kotinis and Parsons 2007a). The experimental hydrodynamic investigation, supported by a CFD analysis and an economic analysis, will be presented at the Annual Society of Naval Architects and Marine Engineers (SNAME) Meeting in Ft. Lauderdale, FL, in November 2007 (Kotinis and Parsons 2007b).

2. Background

The initial Sea Grant supported development of the Ballast-Free Ship Concept was reported in a paper before the Annual Meeting of the Society of Naval Architects and Marine Engineers (SNAME) in Washington, DC, in October 2004 (Kotinis et al. 2004). Overall, the investigation of the Ballast-Free Ship Concept has shown that it provides a viable alternative to the addition of costly ballast water treatment systems in order to meet the evolving performance requirements for ballast water treatment. The concept essentially eliminates the transport of foreign ballast water. This should be more effective than current treatment methods in reducing the potential for the further introduction of nonindigenous aquatic species into the Great Lakes and coastal waters. Furthermore, it should be equally effective as international requirements extend below the 50 micron range (IMO 2004).

The traditional approach to ballast operations, since the introduction of steam machinery, has been the use of water ballast to increase the weight of the vessel in the light cargo condition. A paradigm shift in thinking here views the ballast condition as a change of buoyancy rather than an addition of weight in order to get the vessel to its safe ballast drafts. Such a shift in thinking led to the invention of the Ballast-Free Ship Concept (US Patent #6,694,908 2004).

In this concept, the traditional ballast tanks are replaced by longitudinal, structural ballast trunks that extend beneath the cargo region of the ship below the ballast draft. The arrangement of an equal capacity conventional Seaway-size bulk carrier is shown on the left in Fig. 2.1; the arrangement of a Ballast-Free Ship Concept Seaway-size bulk carrier is shown for comparison on the right. In this example, the three ballast trunks per side are connected to the sea through a plenum at the bow and a second plenum at the stern. Schematic trunk and plenum arrangements at the bow and stern of the vessel are illustrated in Fig. 2.2 and 2.3, respectively. These trunks are flooded with seawater to reduce the buoyancy of the vessel in the ballast condition in order to get the vessel down to its ballast drafts. Since there is a natural hydrodynamic pressure differential created between the bow region and the stern region of a ship due to its motion through the water, a slow flow is induced in these open ballast trunks. This ensures that the ballast trunks are always filled with slowly-moving "local seawater." This should ensure that there is no transport of nonindigenous aquatic species across the globe. Therefore, the vessel becomes foreign "ballast-free" from the traditional viewpoint.

When the ballast voyage is completed, the ballast trunks can be isolated from the sea by valves and then pumped dry using conventional ballast pumps. The need for costly ballast water treatment equipment or ballast water treatment chemicals would, thus, be eliminated. This approach would also be equally effective for biota smaller than 50 microns. During the full load condition or any condition where ballast is not necessary, the double bottom ballast trunks can be segregated utilizing sluice gate valves. This is needed to provide the vessel adequate damage survivability.

In order to provide adequate intact stability, equivalent damage survivability, equivalent cargo capacity, etc., the entire vessel design needs to be developed to support this concept of ballast operations as illustrated in Fig. 2.1. The ship requires a higher tank top in order to locate enough ballast trunk volume below the ballast draft and requires a greater hull depth in order to maintain the vessel's capacity to carry light cargos, such as grain. The Ballast-Free Ship Concept also

includes features to minimize the buildup of sediment within the ballast trunks and facilitate their required cleaning; i.e., easier to clean 2.4 m high ballast trunks and the elimination of the lower part of the floors next to the shell.

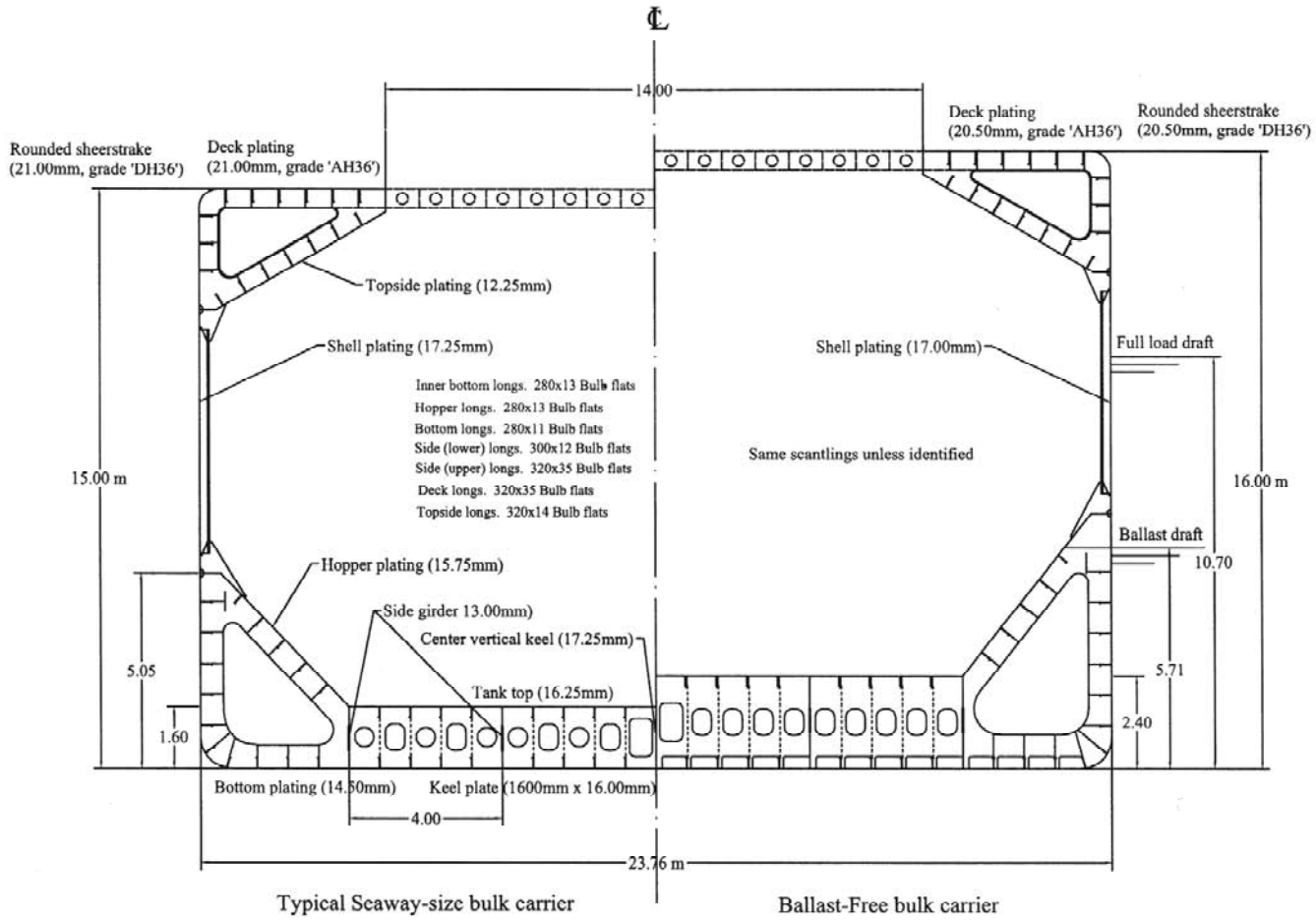

Figure 2.1: Typical Seaway-size Bulk Carrier (left) and Ballast-Free Concept Bulk Carrier (right)

As noted, the initial research on the development of the Ballast-Free Ship Concept was limited by its required comprehensive research scope and limited associated budget. For budgetary reasons, it was only feasible to support model testing that utilized an existing model. Although the vessel type of greatest interest for the Great Lakes nonindigenous aquatic species introduction problem is the Seaway-size bulk carrier, the best available model was of a relatively finer, higher-speed barge-carrying Lighter Aboard Ship (LASH) vessel. This existing model was modified to utilize a more conventional stern, but the model test results were not directly applicable to the Seaway-size bulk carriers studied in detail in the rest of the research effort.

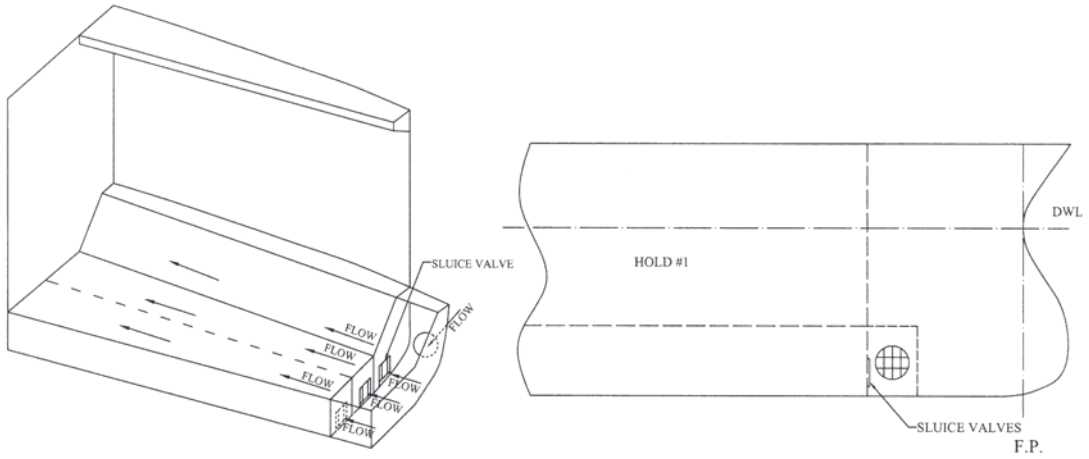

Figure 2.2: Typical Forward Plenum and Collision Bulkhead Arrangement

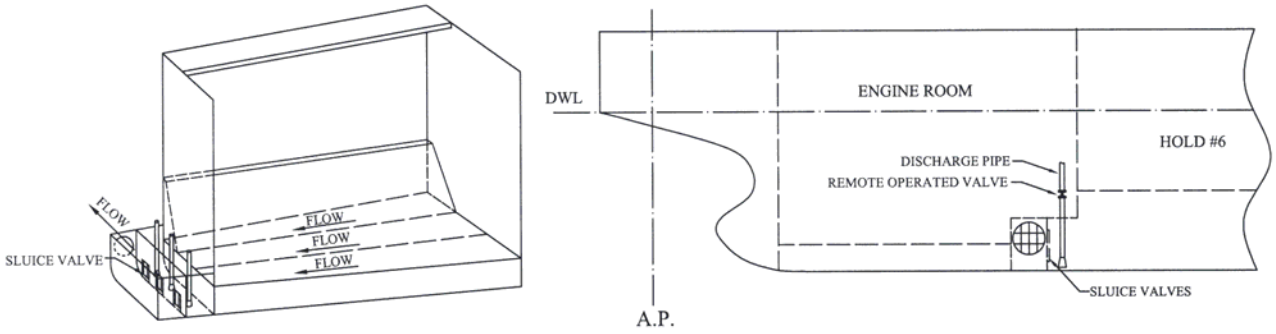

Figure 2.3: Typical Aft Plenum Arrangement

Budget restrictions in the initial investigation phase also required that the model tests be limited to a single system design for the existing model. There was no opportunity to optimize the hydrodynamic design of the system to minimize the economic impact of the Ballast-Free Ship Concept design. Model tests and Computational Fluid Dynamics (CFD) simulations using the modified LASH vessel hull showed that the specific ballast intake and discharge locations and method tested in the initial investigation resulted in a modest 2.2% increase in resistance but a more significant 7.4% increase in the required propulsion power. This specific result assumed a change in the ballast water within the ballast trunks once every two hours, which would meet the environmental intent of the Ballast-Free Ship Concept. The large power increase could result in an undesirable engine size increase and would result in fuel cost penalties. In that investigation, it was concluded that further hydrodynamic optimization could eliminate most, if not all, of this significant added power requirement.

3. Experimental Investigation

The Ballast-Free bulk carrier model, which was designed and built during the initial GLMRI sponsored phase of this project (Parsons and Kotinis 2006), was tested at the University of Michigan Marine Hydrodynamics Laboratory (MHL) in January of 2007. The main particulars of the ship are shown in Table 3.1. The characteristics of the model in the ballast condition are presented in Table 3.2. The bow and the stern of the constructed model are shown in Figs. 3.1 and 3.2, respectively. All the tests were carried out at the ballast drafts at which the Ballast-Free trunks would be in use.

Table 3.1: Main Particulars of the Ballast-Free Bulk Carrier

Waterline length (m)	195.5
Maximum beam (m)	23.76
Depth to main deck (m)	16.00
Full-load draft (m)	10.70
Block coefficient C_B	0.835

Table 3.2: Characteristics of the Ballast-Free Bulk Carrier Model in the Ballast Condition

Geometric scale ratio λ	37.92
Waterline length (m)	5.00
Maximum beam (m)	0.627
F.P. draft @ 40% DWL (m)	0.113
A.P. draft @ 70% DWL (m)	0.198
Wetted surface area (m^2)	5.34

Figure 3.1: Bow View of the Seaway-sized Bulk Carrier Model

Figure 3.2: Stern View of the Seaway-sized Bulk Carrier Model

3.1 Arrangements and Design of Inlet and Outlet Plena

A full-scale diameter of approximately 1 m was chosen for the plena inlet and outlet to ensure a smooth inflow and outflow without imposing severe constraints on the structural arrangements. The corresponding inlet/outlet diameter at model scale is approximately 2.6 cm. The flow rate in the longitudinal trunks was calculated assuming a full-scale volume of ballast water equal to 18,500 m^3. This value was obtained from similar ships, under the assumption of flooding both the normal ballast tanks and a central cargo hold for a heavy weather ballast condition. Assuming an exchange time of 90 min and utilizing Froude scaling, the internal flow rate at model scale is $Q_m = Q_s \, \lambda^{-5/2} = 3.9 \cdot 10^{-4}$ m^3/s. Using the continuity equation and assuming a symmetrical plenum about the centerplane, the average discharge fluid speed is 0.382 m/s.

The selection of the inlet location was based primarily on providing a pressure differential capable of sustaining a steady trunk (internal) flow. In addition to this, the inlet must be adequately submerged to avoid air ingestion and interaction with the free surface and the bow-generated wave system. An important design constraint is the low forward draft in the ballast condition. It was decided to locate the water inlet right on the face of the bulbous bow in the area around the stagnation point to take advantage of the high positive pressure in this region. Therefore, the centroid of the water inlet was placed at approximately 25% of the design waterline (DWL) above the keel as shown in Fig. 3.3. In this way, the water exchange goal of 99% in less than two hours can be reached, or even exceeded (Kotinis 2005). The fluid exchange at the ballast speed of 15.5 knots (assuming no voluntary speed reduction due to heavy weather) can then be achieved in a distance less than 30 nautical miles.

Figure 3.3: Location of Forward Ballast Trunk Inlet

In order to investigate the effect of the water discharge on the flow at the stern, two different discharge locations were selected; one close to Station 17 and one close to Station 19 as shown in Fig. 3.4. Station 17 is approximately at the location of the forward engineroom bulkhead in the full-scale ship; Station 19 is approximately at the aft engineroom bulkhead. The discharge at Station 17 was located about the 45% DWL and the discharge at Station 19 was located at about the 30% DWL. The flow was discharged at about 10 degrees to the local hull surface. In this way, the effect on the boundary layer flow, as well as the effect on the propeller inflow, could be investigated in a systematic manner.

The choice of the discharge locations investigated was based on the results of a numerical CFD investigation of the stern flow. These results are presented in the next section. If trunk flow rate maximization were the only criterion, the water outlet should be located in an area with high suction pressure to maximize the pressure differential. On the other hand, when the propeller operation is taken into account, the objective is to minimize the power requirement subject to achieving adequate ballast trunk flow.

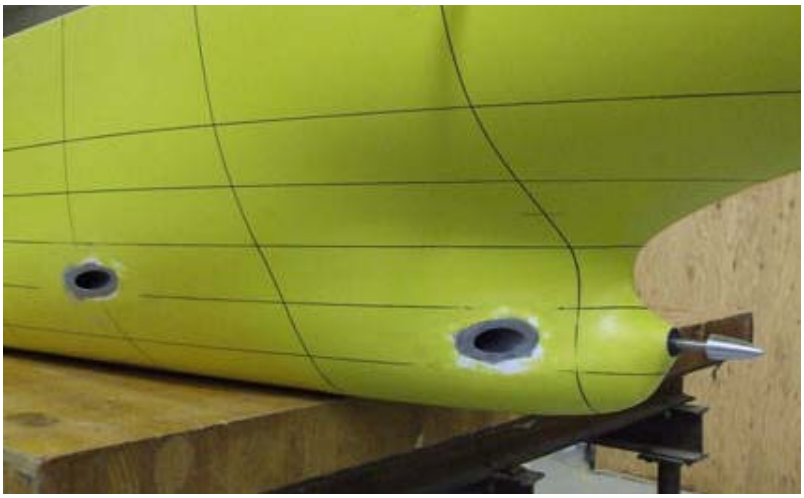

Figure 3.4: Location of Two Ballast Trunk Discharges Investigated

3.2 Experimental Setup

Because the modeling of the internal flow trunks could not be reliably scaled at the small model scale utilized, the scaled total trunk flow was pumped rather than using natural flow. The trunks were modeled by a 1-inch internal diameter pipe that was connected to the water suction at the bow and the water discharge at the stern. The steady internal flow was created and maintained by a flexible-impeller pump. The flow rate was controlled by a high-precision needle valve and monitored by a flow meter. The flow was diverted to the selected discharge location and subsequently split to provide a symmetric water discharge at the stern of the model. Details of the internal flow model are shown in Figs. 3.5 and 3.6.

Figure 3.5: Internal Flow Arrangements in the Bow Region

Figure 3.6: Internal Flow Arrangements in the Stern Region – Looking Forward

3.3 Resistance Tests

The experimental test plan for both the resistance and propulsion tests is shown in Table 3.3. It was decided to test a range of speeds spanning a typical ballast condition operating range of bulk carriers of this size. The speed of 15.5 knots is considered as the designed ballast speed for purposes of flow scaling.

Table 3.3: Experimental Test Plan

Test speed	Ship speed (knots)	Model speed (m/s)	Froude number
1	14.50	1.210	0.173
2	15.50	1.295	0.185
3	16.50	1.378	0.197

The resistance of the Ballast-Free bulk carrier model was measured and then extrapolated to full scale using the ITTC-recommended method (ITTC 1978). The results for the full scale resistance and effective power are presented in Figs. 3.7 and 3.8, respectively. For all testing conditions, the results are reported at a standard temperature of 15°C. Prior to the resistance tests, a static calibration test of the load cell was performed. Additional resistance tests were performed at low speeds to derive the form factor used in the extrapolation procedure. Errors related to the static calibration and the form factor derivation were considered as sources of bias error. Four different measurements were obtained at each speed shown in Table 3.3 in order to minimize the precision error. The total uncertainty is calculated as the root sum square of the total bias error and the total precision error. The error bands shown in Figs. 3.7 and 3.8 correspond to the computed uncertainty values, assuming a 95% level of confidence.

The water discharge at the stern has a negative effect on ship resistance in both cases, even though the discharge at Station 17 seems to exacerbate the resistance increase. Even though the resistance curves plotted in Fig. 3.7 show an increase in the average values, the difference with respect to the baseline case is not statistically significant as seen by the overlapping error bands.

3.4 Propulsion Tests

The resistance tests were followed by a series of propulsion tests using the MHL stock model propeller No. 23. The No. 23 stock propeller was the available propeller providing the highest propulsive efficiency and, at the same time, satisfying the hull clearance requirements, assuming a full-scale propeller diameter of 6.0 m. The propeller characteristics for the No. 23 model propeller are shown in Table 3.4. The non-dimensional thrust and torque coefficients plotted versus the coefficient of advance (Kt, Kq – J) of the No. 23 model propeller are shown in Fig. 3.9. The thrust and torque measurements at the self-propulsion condition at each speed were analyzed using the ITTC-recommended method (ITTC 1978). The calculated required delivered power is shown in Fig. 3.10. An uncertainty analysis was also performed for the propulsion test results giving the error bands shown.

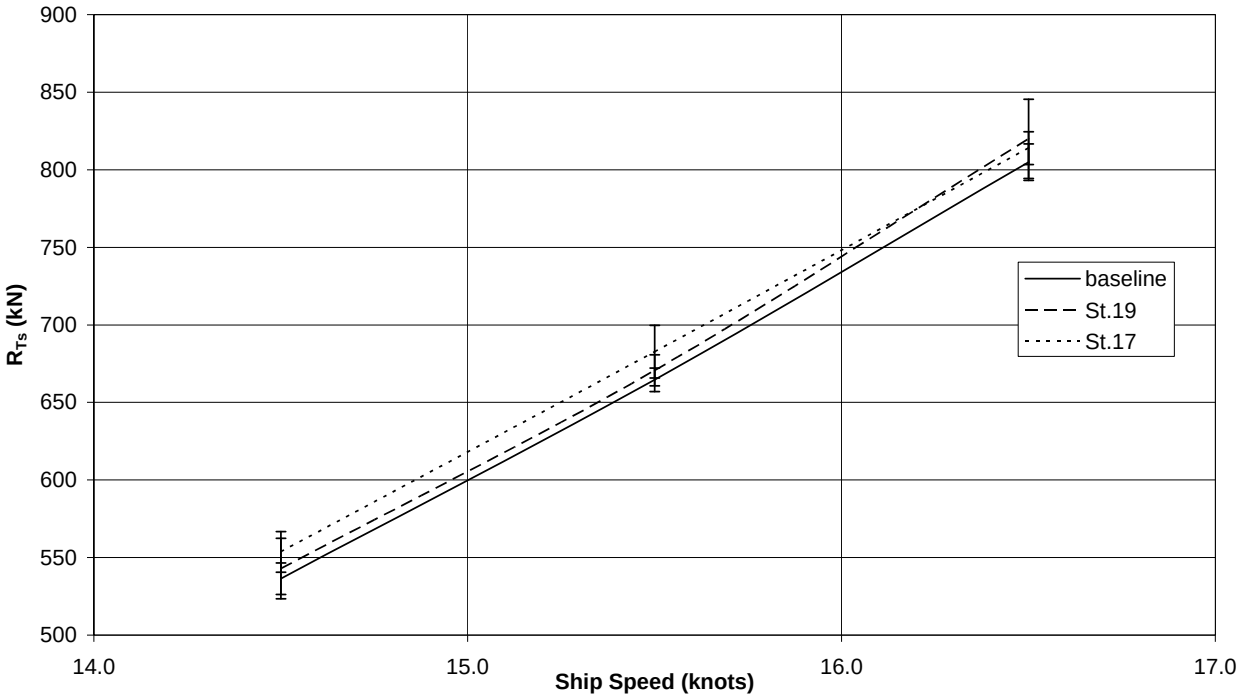

Figure 3.7: Ballast-Free Bulk Carrier Total Resistance

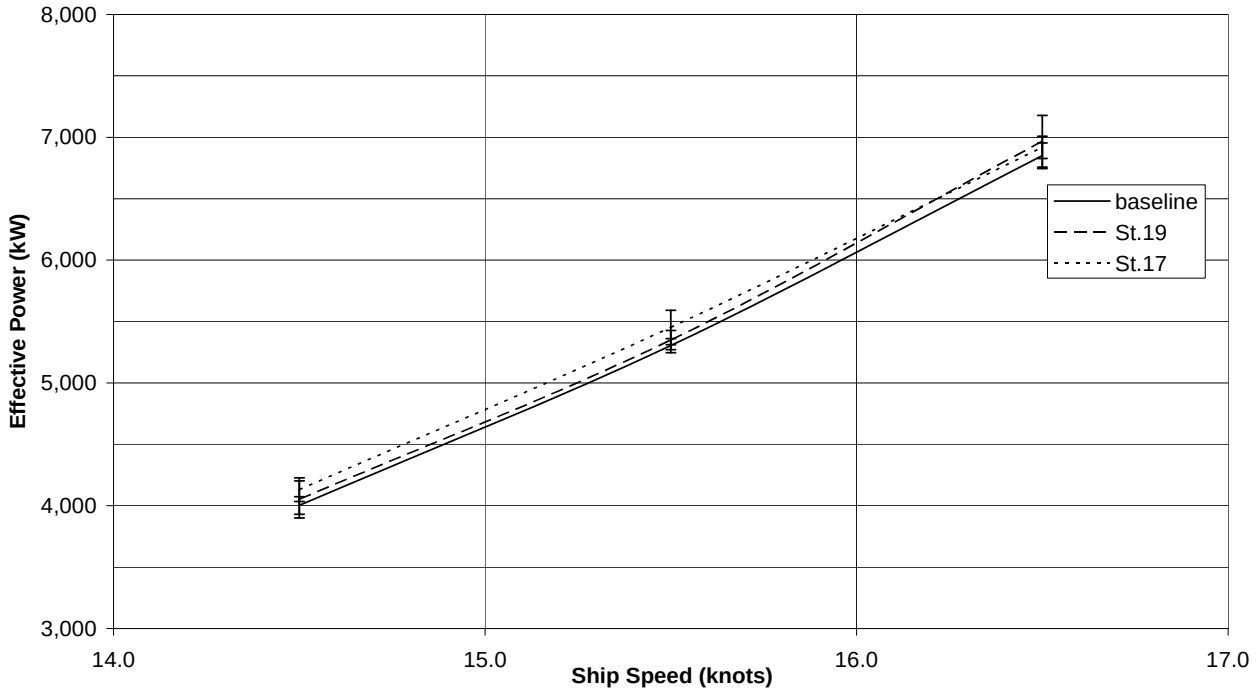

Figure 3.8: Ballast-Free Bulk Carrier Total Effective Power

Table 3.4: Characteristics of the MHL No. 23 Stock Propeller

Number of blades	4
Diameter D_p (m)	0.158
Hub diameter (m)	0.031
Pitch-diameter ratio P/D_p	1.08
Expanded area ratio A_e/A_o	0.55

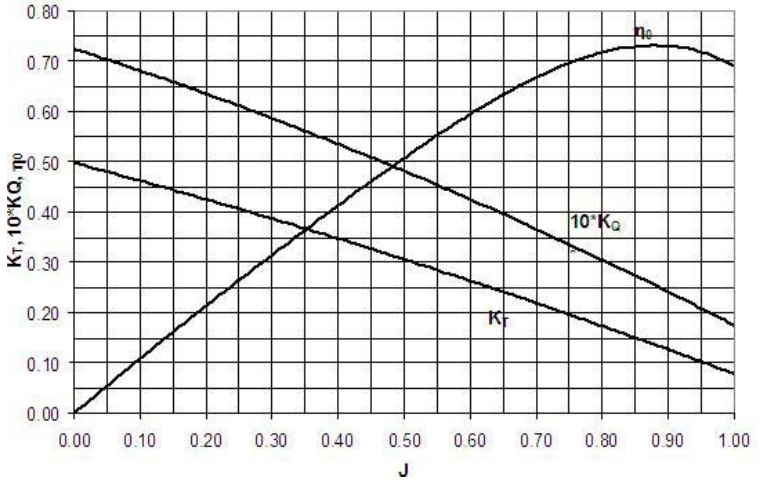

Figure 3.7: Propeller Coefficients versus Advance Coefficient

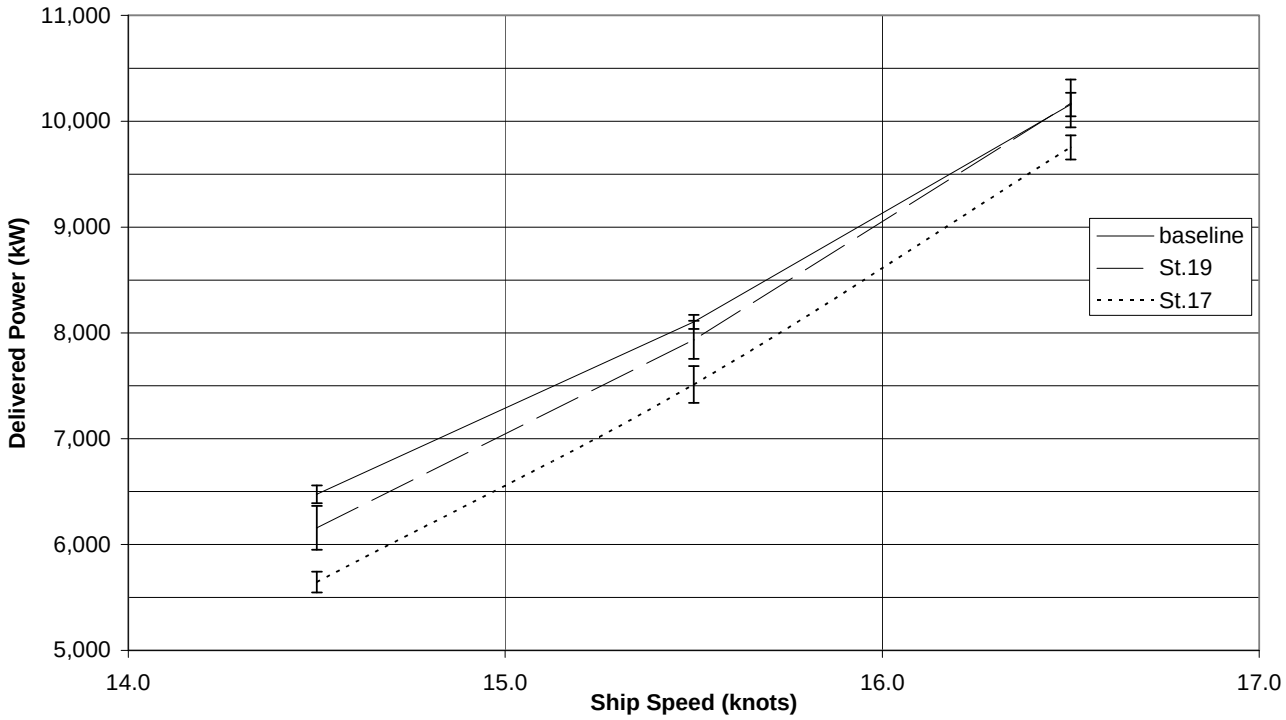

Figure 3.10: Ballast-Free Bulk Carrier Required Delivered Power

The propulsion test results depicted in Fig. 3.10 show a noteworthy reduction in the powering requirements caused by the water discharge at the stern. At a ballast condition speed of 15.5 knots, the reduction in the required delivered power is 7.3% for the discharge close to Station 17 and 2.1% for the discharge close to Station 19. Note that this is compared with a required delivered power increase of 7.4% observed in the initial investigation with the modified LASH vessel and the initial discharge configuration. A physical interpretation of this outcome cannot be fully explained without a detailed analysis of the change in the effective wake entering the propeller with the trunk discharge and its interaction with the detailed propeller design. In the current phase of the project, a qualitative analysis of the results was attempted by utilizing CFD and analyzing the hull nominal wake. This analysis is presented in the next section. An additional advantage of fitting the preferred discharge location near Station 17, at least from an engineroom arrangements perspective, is that the ballast trunks would not have to be carried through the engineroom.

3.5 Propeller Efficiency

Because a stock propeller was used in the experimental investigation, it was unclear to what extent the propulsion power reduction found would actually be realized if an optimum propeller design had been used on the model. The stock propeller utilized in the propulsion tests has characteristics quite similar to those of the standard Wageningen B-Screw Series B4-55 propeller (van Lammeren et al. 1969). Therefore, an attempt was made to find the optimum, in terms of efficiency, standard B-Screw Series propeller and compare its performance with the stock propeller utilized. In this manner, the margin of efficiency improvement of the stock propeller used could be estimated. This could help clarify whether the utilization of an optimum propeller could have benefited as much as the stock propeller from the ballast trunk discharge effect. The results of the analysis for the optimum B-Screw Series propeller the ballast speed of 15.5 knots are shown in Table 3.5.

Table 3.5: Determination of Optimum B4-55 Wageningen B-Screw Series Propeller

P/D_p	η_B	*n (rpm)*	σ	τ_c	*Back Cavitation (%)*	*J*
0.5	0.510	137	0.368	0.100	0.5	0.321
0.6	0.543	121	0.473	0.131	1.0	0.364
0.7	0.555	108	0.582	0.166	1.5	0.405
0.77	0.558	102	0.659	0.191	2.2	0.433
0.8	0.556	99	0.693	0.202	2.5	0.444
0.9	0.551	92	0.804	0.241	3.5	0.480
1.0	0.541	86	0.915	0.282	4.5	0.513
1.08	0.532	81	1.023	0.324	5.5	0.545
1.2	0.517	77	1.128	0.368	6.5	0.574
1.3	0.506	73	1.231	0.413	7.5	0.601
1.4	0.497	70	1.330	0.460	8.5	0.627

The results in Table 3.5 show that a 4-bladed propeller with a pitch-diameter ratio of 0.77 provides the optimum efficiency $\eta_B = 0.558$ with an acceptable extent (2.2%) of back cavitation.

A comparison of the efficiency of two B-Screw propellers with the model stock propeller in the three test conditions (no ballast trunk flow or baseline and discharge at Stations 17 and 19) is shown in Table 3.6.

Table 3.6: Propeller Efficiency η_B

MHL No.23 Propeller – baseline	0.556
MHL No.23 Propeller – Station 17	0.565
MHL No.23 Propeller – Station 19	0.558
B4-55 (P/D_p = 1.08, same as No. 23)	0.532
Optimum B4-55 (P/D_p = 0.77)	0.558

These results reveal that an improvement in propeller efficiency when operating behind the ship hull of about 4.9% (from 0.532 to 0.558) might be achieved by utilizing an optimum propeller. On the other hand, a different picture is observed when the ballast trunks are discharging at the stern. The propeller efficiency is slightly increased when discharging close to Station 19 and more significantly increased (1.6%) when discharging close to Station 17. Therefore, it can be argued that an optimum propeller will probably not benefit quite as much, in terms of propeller efficiency, as the stock propeller utilized.

However, a significant part of the overall propulsive efficiency improvement can be attributed to the increase of the hull efficiency, as shown in Table 3.7. Thus, it appears that most of the required power improvement (actually a small apparent resistance increase and a 7.3% delivered power reduction) observed would still be realized when an optimum propeller were used.

Table 3.7: Hull Efficiency and Propulsive Efficiency

	Hull Efficiency, η_H	Propulsive Efficiency, $\eta_P = \eta_B * \eta_H$
MHL No.23 Propeller – baseline	1.194	0.664
MHL No.23 Propeller – Station 17	1.286	0.727
MHL No.23 Propeller – Station 19	1.214	0.677

4. Numerical Investigation

The commercial CFD software FLUENT® (Fluent 2006) was utilized to study the external flow around the bulk carrier model. The numerical study was greatly facilitated by utilizing a predominantly hexahedral grid to model the flow domain around the hull of the vessel. A 'double-body' flow model, which does not take the free-surface flow into account, was adopted considering the free surface as a plane of symmetry. This particular grid, shown in Fig. 4.1, allowed a better resolution of the flow inside the boundary layer; thus, providing more accurate results with respect to the mixing of the discharged water (blowing) and the boundary layer flow. The total number of cells was 1,019,973. The grid generation was performed with the aid of Gridgen® (Gridgen 2007).

4.1 Description of the Numerical Solver

The numerical solver of FLUENT is based on a finite-volume method with the flow properties calculated at the cell centers. The fluid velocity is obtained by solving the Reynolds-Averaged Navier-Stokes (RANS) equations. The diffusion terms in the RANS equations are discretized with a central differencing scheme. The convection terms are discretized using a higher-order upwind scheme to minimize numerical diffusion. The discretized equations are solved using the Gauss-Seidel iterative algorithm. The solution convergence is accelerated through the utilization of an algebraic multi-grid method. Further details of the numerical methods can be found in (Mathur and Murthy 1997) and (Kim et al. 1998).

The turbulence model utilized in the computations was the shear-stress transport (SST) model (Menter 1994). This model implements a blending function in order to apply the standard k - ω model close to solid boundaries (ship hull) and a transformed version of the k - ε model in the far field. A low-Reynolds-number version of the k - ω model was employed. The SST model has been shown to provide quite accurate results for ship flows (Kim and Rhee 2002, Duvigneau et al. 2002).

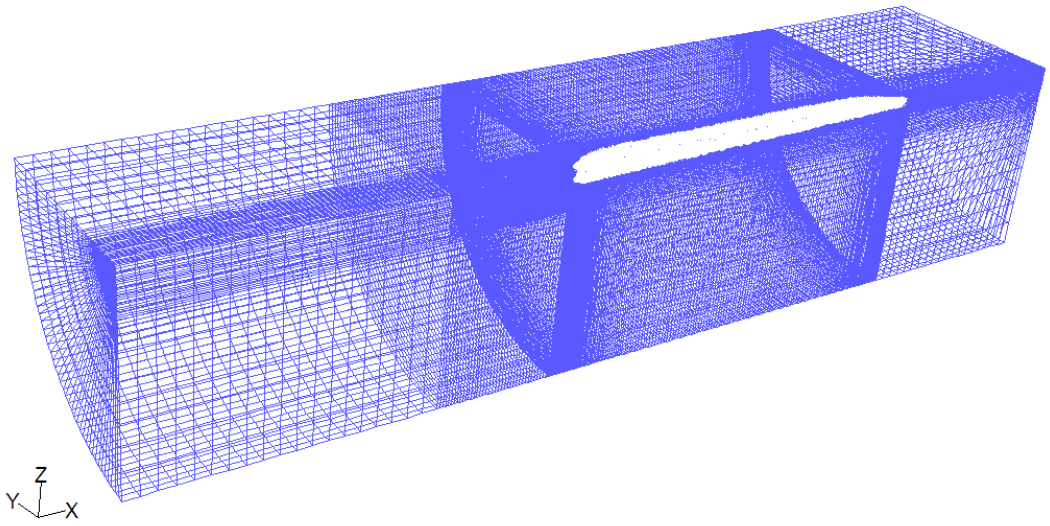

Figure 4.1: Computational Grid for the Ballast-Free Bulk Carrier

4.2 Numerical Investigation Results

Computations were performed for the Ballast-Free bulk carrier model in the ballast condition, where the model-scale speed is 1.295 m/s and the corresponding Reynolds number (in fresh water at 15°C) is 6.10e+6. The pressure coefficient contours at the bow of the Ballast-Free bulk carrier model in the ballast condition are shown in Fig. 4.2. The positive pressure area at the bow extends up to approximately 7% of the ship length aft of the forward perpendicular (FP); thus, the available locations for the inlet of the bow plenum are limited. This corroborates our decision to place the water inlet at the center of the bulbous bow. The corresponding pressure coefficient contours at the stern are presented in Fig. 4.3. Suction pressure exists over the parallel section and most of the ship stern. Between Stations 17 and 18 ($0.85 \leq x/L_{PP} \leq 0.90$) and close to the free surface, a low suction pressure region exists. The latter interacts with the suction pressure peak that exists close to the keel at Station 18 ($x/L = 0.90$) and produces a considerable girthwise pressure gradient. The end result is the formation of a streamwise vortex, which moves downstream and crosses the propeller plane.

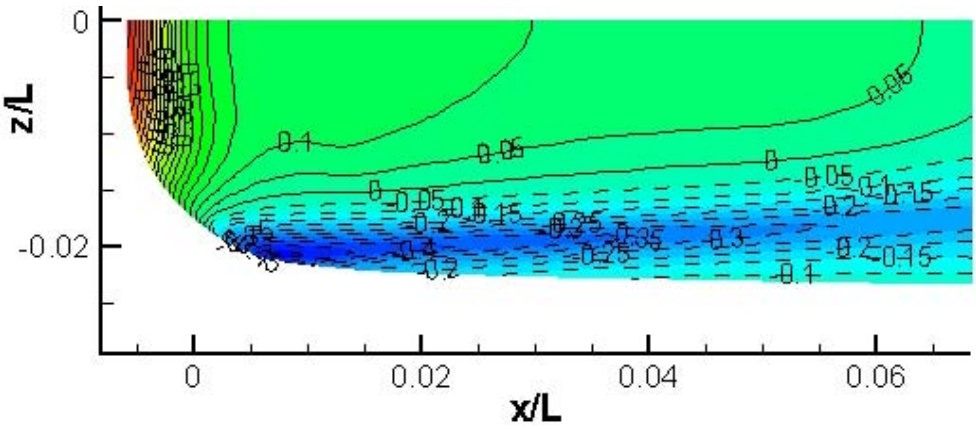

Figure 4.2: Bow Pressure Coefficient Contours

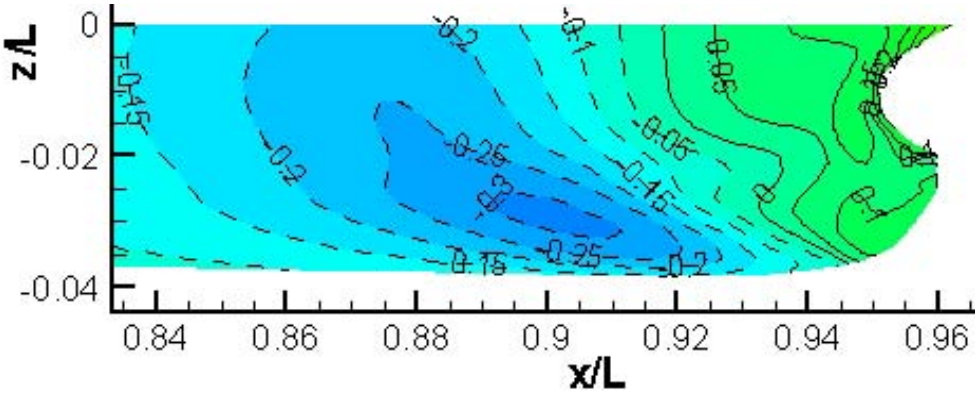

Figure 4.3: Stern Pressure Coefficient Contours

4.3 Numerical Investigation of the Water Inlet at the Bow and the Water Discharge at the Stern

The effect of the water suction at the end of the bulbous bow and the water discharge close to Station 17 on the flow around the model was investigated numerically using FLUENT®. The discharge flow direction was set to 10° with respect to the surface tangent to avoid obstructing the boundary layer flow. A smaller angle would probably be infeasible to implement in model or full scale. The major modeling requirement was to provide adequate grid resolution close to the hull to account for the interaction between the boundary layer flow and the trunk inflow and outflow. For this purpose, a slightly modified version of the original grid shown in Fig. 4.1 was utilized. The modifications were limited to the modeling of the region close to the inlet and discharge locations. In this case, the total number of cells was increased to 1,074,580.

The pressure coefficient contours with the water inlet at the bow are shown in Fig. 4.4. A comparison with the pressure coefficient contours in Fig. 4.2 reveals that the positive pressure levels increase in the vicinity of the water inlet, even though this effect vanishes downstream, of x/L = 0.02. The pressure coefficient contours at the stern are shown in Fig. 4.5. A small reduction in suction pressure, relative to the pressure distribution shown in Fig. 4.3, is observed slightly upstream of the discharge location. The opposite effect is observed slightly downstream. The net effect on the pressure force is shown to be minimal. However, these observations do not take into account the effect on the propeller inflow and the interaction between propeller and hull. Based on the results shown in Table 3.7, this interaction seems to be significantly affected by the water discharge at the stern.

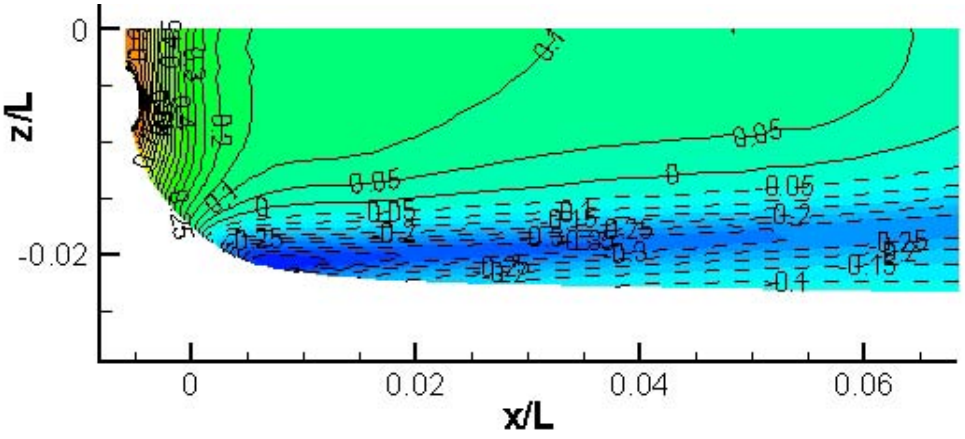

Figure 4.4: Bow Pressure Coefficient Contours – Water Inlet

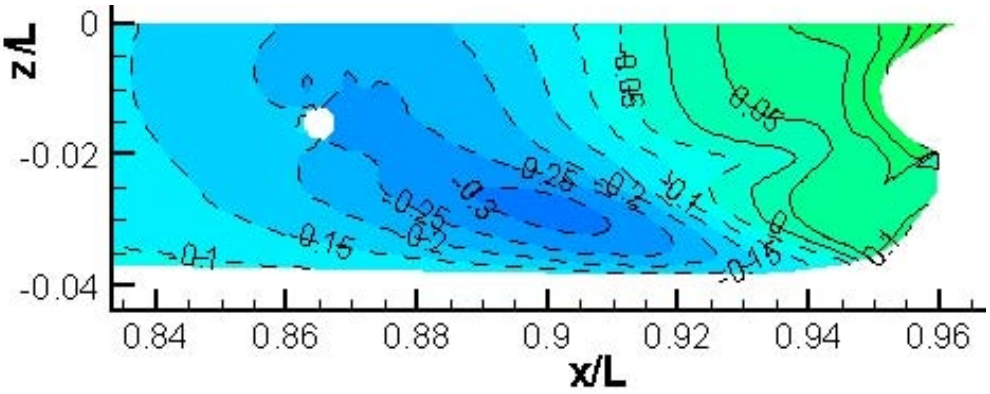

Figure 4.5: Stern Pressure Coefficient Contours – Water Discharge

4.4 Numerical Investigation of the Water Discharge Effect on the Model Hull Nominal Wake

As a first step in investigating the water discharge effect on the propulsion of the vessel, the effect of the water discharge on the nominal wake of the model hull was investigated. A qualitative measure of propulsive performance improvement and also vibration reduction is the uniformity of the nominal wake field in the propeller disk. Increased nominal wake uniformity can be obtained through the introduction of water into the flow deficit region in the upper half of the propeller disc and the interaction of the discharged flow with the longitudinal bilge vortex formed at the stern of the vessel. This interaction can be optimized by selecting the appropriate discharge location. A single-objective optimization problem can be formed with the wake uniformity in the propeller disk as the objective function. This analysis, even though based on a simplistic criterion, can serve a twofold purpose: first, to verify the potential for increased wake uniformity through an optimum discharge location and, second, to shed some light on the stern flow physics.

In order to minimize the computational time in this parametric study, the flow was restricted to the aft part of the vessel. This enabled investigation of the stern flow with a more refined grid. The flow domain was truncated by removing the bow and part of the ship parallel mid-body. The total number of cells in this case was 519,750. The plane at Station 14 ($x/L_{PP} = 0.70$) was considered as the new flow-inlet boundary. The velocity components and the turbulence characteristics at this plane were set equal to the corresponding profile obtained from the converged full-length hull solution. The position of the discharge location, the coordinates of the centroid of the trunk flow outlet, was considered as the problem variable. Bounds on the problem variables were set by considering operational and design constraints. The longitudinal coordinate range was between 85%L_{PP} (Station 17) and 94%L_{PP} (slightly forward of Station 19), which correspond roughly to the engineroom forward and aft bulkhead. The vertical coordinate of the centroid was limited to the range between 25 and 45%DWL, measured upward from the baseline.

A complete factorial design was utilized for the numerical simulations; three equi-spaced positions in the longitudinal direction (85, 89.5 and 94% L_{PP}) and two in the vertical direction (25 and 45% DWL) were used. This complete factorial design is also a mixed orthogonal array of strength 2 capable of capturing the main effects of each variable (Hedayat et al. 1999). The

goal was to sample the domain in such a way that it would facilitate the building (training) of an Artificial Neural Network (ANN)-based metamodel to be utilized in the optimization phase.

The numerical investigation results are presented in Table 4.1. These results reveal that a slightly more uniform wake in the propeller disk can be obtained by discharging closer to the bilge. In addition to this, a reduction of the standard deviation of the axial velocity (σ_{Vax}) by approximately 2% in comparison to the no-discharge-flow (initial) case can be achieved by discharging at x/L = 0.895 (slightly forward of Station 18).

Table 4.1: Standard Deviation of Axial Velocity in the Propeller Disk

Case ID	*x (%L_{BP})*	*z (%DWL)*	*σ_{Vax} (m/s)*
Initial	-	-	0.157
1	85.0	25	0.159
2	85.0	45	0.158
3	86.5	35	0.159
4	88.0	25	0.157
5	88.0	45	0.160
6	89.5	25	0.154
7	89.5	45	0.160
8	92.5	35	0.156
9	94.5	25	0.157
10	94.5	45	0.161

Contours of axial vorticity at different stations along the vessel hull as well as contours of the axial velocity inside the propeller disk are shown in Figs. 4.6 and 4.7. The contour plots in Fig. 4.6 reveal that water discharge near the bilge (i.e. case no. 6) causes a stretching of the vortex in the transverse direction. On the other hand, water discharge at a higher vertical position causes a stretching of the vortex in the vertical direction and a slight contraction in the transverse direction. The stretching of the vortex in the transverse direction explains the increased uniformity of the wake in the propeller disk. As shown in Fig. 4.7, a larger part of the longitudinal bilge vortex appears to pass through the propeller disk in case no. 6 compared with the two other cases. The bilge vortex collects frictional wake from the ship boundary layer. By delivering the frictional wake to the propeller disk, it facilitates the recovery of the axial kinetic energy produced by the ship (Dyne 1995).

An optimum discharge location was found by utilizing a real-parameter Genetic Algorithm (GA) (Deb 2001). Ranking selection was used as the survival operator in a similar manner as the roulette operator is utilized in simple binary GAs. Crossover and mutation operators were utilized in a modified form appropriate for bounded variables encoded in real-parameter chromosomes. Specifically, the simulated binary crossover (SBX) operator adjusted for bounded variables (Deb and Agrawal 1995, Deb 2000) was utilized with a crossover rate of 0.7 and a distribution index of 2. The parameter-based mutation operator (Deb and Goyal 1996), adjusted for bounded variables (Deb 2000), was also employed for the genetic operations. The mutation rate was set to a value of 0.5. An elite-preserving operator was added to the optimizer by carrying the best two solutions over to the next generation.

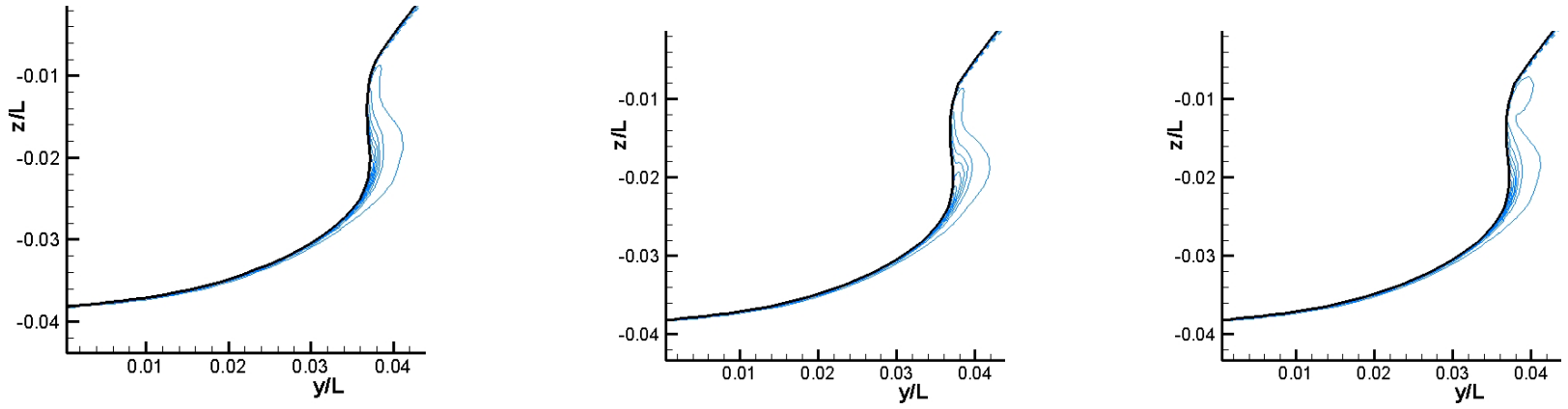

Figure 4.6: Axial Vorticity Contours at $x/L_{PP} = 0.92$, Initial Case (left), Case no. 6 (center) and Case no. 7 (right)

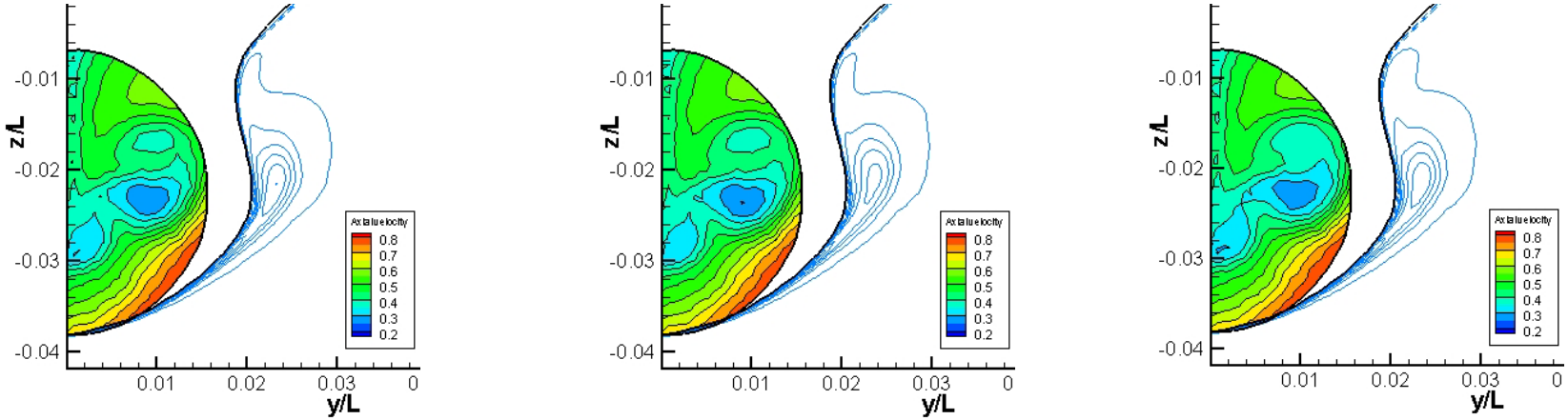

Figure 4.7: Axial Vorticity Contours at $x/L_{PP} = 0.95$ and Axial Velocity (nondimensional) Contours in Propeller Disk, Initial Case (left), Case no. 6 (center) and Case no. 7 (right)

The optimization procedure requires multiple evaluations of the objective function at points within the bounded variable space. In the current research, a surrogate model using an Artificial Neural Network (ANN) was created in order to approximate the nonlinear objective function and eliminate the costly numerical . A network based on sigmoidal logistics activation functions was developed using an input layer with two nodes; two hidden layers each consisting of three nodes, and a single-node output layer. The back-propagation algorithm (Rumelhart et al. 1986) was utilized for training of the network. A learning rate of 0.2 was used for the hidden layers and a rate of 0.1 for the output layer. The update of the network weights was performed only after all training data points were presented to the network ("per-epoch" learning). Momentum terms were added to the learning algorithm to achieve a more stable training procedure.

The discharge location that minimized the objective function within the bounded variable space was centered at x/L = 0.915 and z/DWL = 0.25. The corresponding standard deviation of the axial velocity in the propeller disk was 0.152 m/s. This value provides a 3.2% reduction compared to the initial case without the trunk flow discharge. A comparison between the initial case and the optimum case is shown in Fig. 4.8. In the optimum case, the improvement in wake uniformity due to the water discharge, especially in the upper propeller plane, is apparent.

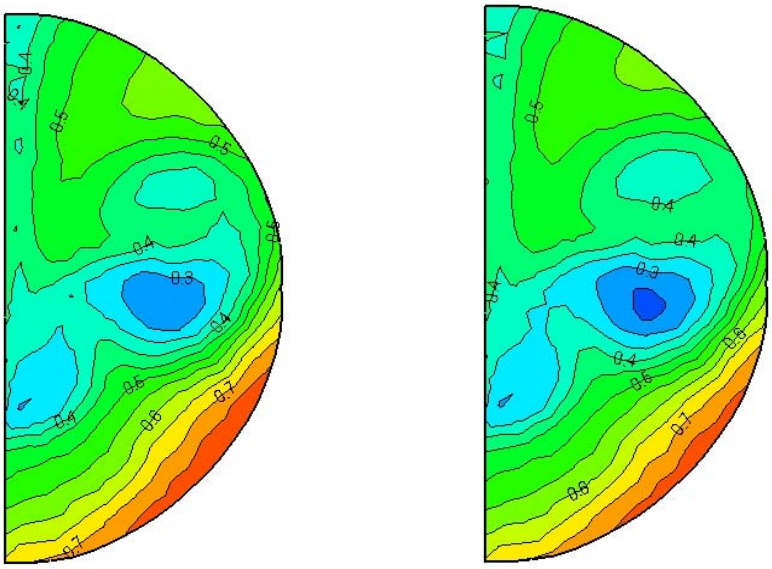

Figure 4.8: Axial Velocity Contours in Propeller Disk, Initial Case (left), Optimum Case (right)

5. Potential Economic Impact of the Research Results

The economic impact of the Ballast-Free Ship concept on the capital and operating cost of a typical Seaway-sized bulk carrier was estimated in a manner similar to that used in the initial investigation of the concept (Kotinis et al. 2004). The results for the water discharge close to Station 17 and close to Station 19 are presented in Fig. 5.1. A realistic scenario was adopted for the economic analysis: a handy-sized bulk carrier transporting grain from the upper Great Lakes (e.g. Duluth, Thunder Bay) to ports in Northern Europe and occasionally transporting steel into the Great Lakes. A North Atlantic voyage route between Rotterdam and Montreal, entering the Great Lakes through the St. Lawrence Seaway while in a ballast condition, is assumed.

A major, conservative assumption is that the 2.1% and 7.3 % reductions in the required power of the Ballast Free bulk carrier will not be enough to permit a change in the main engine; thus, no propulsion machinery capital cost reduction is included. Foreign new construction, typical of Korea, was assumed for the calculation of the hull steel and other construction costs. The eliminated ballast water treatment system was assumed to consist of automatic backflush filtration as a primary treatment combined with UV irradiation for a secondary treatment. The estimated cost of this treatment equipment was based upon a study commissioned by the Great Lakes Ballast Technology Demonstration Project (Hurley et al. 2001).

The net savings in terms of the ΔRFR with the ballast trunk water discharge close to Station 17 is estimated to be about \$0.93 per ton of cargo. The corresponding savings with the water discharge close to Station 19 is estimated to be about \$0.44 per ton of cargo. These savings are relative to the use of filtration primary and UV secondary ballast water treatment when ballast water exchange is no longer permitted in the future.

Vessel data and trip scenario	*Typical bulk carrier*	*Ballast-free bulk carrier*		*Comments*
		Discharge at St.17	*Discharge at St.19*	
Round-trip distance (nautical miles)	6,280			Montreal (CAN) to Rotterdam (NL) through the Seaway
Service speed (kts)	14.5			Typical data for an ocean-going Handymax bulk carrier transporting grain cargo from the Great Lakes (Duluth, Thunder Bay) to ports in Northern Europe and occasionally transporting steel into the Great Lakes.
Speed in ballast condition (kts)	15.5			
Proportion of miles in ballast (%)	35			
Average loaded cargo / maximum cargo (%)	90			
Load factor (%)	58.5			
Days of navigation through the Great Lakes	8			Passage up through the Great Lakes towards the western end
Port days per round trip	14			Includes loading/unloading time, bunkering time, and time waiting for berth
Round trips per annum	7			
Maximum payload (metric tons)	32,000			
Cargo carried per annum (metric tons)	131,000			
Engine nominal MCR (kW)	8,580			Data for the MAN B&W 6S50MC two-stroke engine
Block coefficient	0.835	0.841		Compensate for increased hull steel weight and lost buoyancy at plena
Hull steel weight (metric tons)	5,550	5,770		
Hull steel cost ($)	2,220,000	2,308,000		Assuming a steel price of $400/metric ton
Continuous service rating in ballast condition (kW)	7,700	7,140	7,540	Includes 15% sea margin and effect of change in C_B value
Continuous service rating in full load condition (kW)	7,700	7,155	7,555	Includes 15% sea margin and effect of inlet/outlet hull openings and change in C_B value
Specific fuel consumption (g/(kW*hr))	168.7	166.4	168.0	Data for the MAN B&W 6S50MC engine, ISO ambient conditions
Annual heavy fuel cost ($)	1,039,000	951,000	1,014,000	Fuel price (IFO380) of $270/metric ton, transatlantic part of trip only
Changes in capital cost				
Additional hull steel cost ($)	88,000			
Sluice gates cost ($)	260,000			Acquisition cost plus labor for 52 450x600 mm sluice gates (@ $5,000 each)
Elimination of ballast tank valves ($)	-14,000			14 @ 1,000 each
Reduction in ballast piping cost ($)	-314,000			Removal of main ballast headers (material plus labor)
Reduction in welding cost ($)	-9,500			Reduced welding at the bottom of solid floors (material plus labor)
Additional ballast piping cost ($)	79,000			Addition of ballast piping for F.P. tank (material plus labor)
Additional welding cost ($)	2,600			Additional welding due to raise of inner bottom (material plus labor)
Elimination of ballast water treatment system ($)	-375,000			Assuming automatic backflush filtration combined with UV irradiation
Changes in operating cost				
	Discharge at St.17	***Discharge at St.19***		
Change in heavy fuel oil cost ($)	-88,000	-25,000		
Net capital cost change ($)	-282,900			
Net operating cost change per annum ($)	-88,000	-25,000		
Capital recovery factor	0.1175			i = 10%, n = 20 years
Change in required freight rate ($/metric ton)	-0.93	-0.44		savings

Figure 5.1: Economics Summary Comparing a Typical Bulk Carrier with Filtration and UV Treatment with Ballast-Free Bulk Carrier with Two Different Discharge Locations

6. Dissemination of Study Results

The following publications were related to this funded research:

- Parsons, M. G., "Ballast-free ships: Investigations at the University of Michigan use local water for ballast," *Great Lakes Seaway Review*, **35**-2: 19 & 21, January-March, 2007.

- Kotinis, M. and Parsons, M. G. 2007a "Numerical Investigation of the Flow at the Stern of a Ballast-Free Bulk Carrier Model" *Proceedings* of the 9th Int. Conference in Numerical Ship Hydrodynamics, Aug. 2007.

- Kotinis, M. and Parsons, M. G., "Hydrodynamic Optimization of the Ballast-Free Ship Concept" to appear in *Transactions* SNAME, **115**, 2007.

- A *University Record* article is under preparation by the University of Michigan News Services.

The following presentations were related to this funded research:

- Parsons, M. G. and Kotinis, M., "Hydrodynamic Optimization of the Ballast-Free Ship Concept," presented at the 50th Annual Conference on Great Lakes Research, International Association for Great Lakes Research, May 31, 2007, University Park, PA.

- Kotinis, M. and Parsons, M. G., "Hydrodynamic Optimization of the Ballast-Free Ship Concept" to be presented at the Society of Naval Architects and Marine Engineers Annual Meeting, Ft. Lauderdale, FL, Nov. 2007.

- A ~5 min. video is under preparation by the University of Michigan News Services.

The results of the funded research were reviewed in the following class:

- The results of this investigation were presented in the graduate class NA570 Advanced Marine Design at the University of Michigan in the Winter Semester 2007.

This page intentionally left blank.

7. References

Ballast Water News (2004) "The Ballast-Free Ship - Fact or Fancy?" *Ballast Water News*, Global Ballast Water Management Program, IMO, **17**, April-June.

Deb, K. 2000 "An efficient constraint handling method for genetic algorithms," *Computer Methods in Applied Mechanics and Engineering*, **186**, 2-4, pp. 311-338.

Deb, K. 2001 *Multi-Objective Optimization using Evolutionary Algorithms*, John Wiley.

Deb, K. and Agrawal, R.B. 1995 "Simulated binary crossover for continuous search space," *Complex Systems*, **9**-2, pp. 115-148.

Deb, K. and Goyal, M. 1996 "A combined genetic adaptive search (GeneAS) for engineering design," *Computer Science and Informatics*, **26**-4, 1996, pp. 30-45.

Duvigneau, R., Visonneau, M. and Deng, G.B. 2002 "On the Role Played by Turbulence Closures in Hull Shape Optimization at Model and Full Scale," 24th Symposium on Naval Hydrodynamics, Fukuoka, Japan, August 8-13.

Dyne, G. 1995 "The Principles of Propulsion Optimization," *Transactions RINA*, **137**, pp. 189-208.

Fluent 2006 "FLUENT 6.3 User's Manual," Fluent Inc., Lebanon, NH.

Gridgen 2007 "Gridgen 15.1 User Manual," Pointwise Inc., Fort Worth, Texas.

Hedayat, A.S., Sloane, N.J.A., and Stufken, J. 1999 *Orthogonal Arrays: Theory and Applications*, Springer Series in Statistics, Springer-Verlag, New York, pp. 247-315.

Hurley, W. L. JR., Schilling, S. S. JR. and Mackey, T. P. 2001 "Contract Designs for Ballast Water Treatment Systems on Containership *R. J. Pfeiffer* and Tanker *Polar Endeavor*," SNAME/ ASNE Marine Environmental Engineering Technical Symposium, Arlington, VA, May 31-June 1 (CD).

IMO 2004 "International Convention for the Control and Management of Ships' Ballast Water & Sediments," Diplomatic Conference, February, London.

ITTC 1978 "15th International Towing Tank Conference, 3-10 September 1978, The Hague, The Netherlands", Netherlands Ship Model Basin, Wageningen.

Kim, S.E., Mathur, S.R., Murthy, J.Y., and Choudhury, D. 1998 "A Reynolds-Averaged Navier-Stokes Solver using Unstructured Mesh-Based Finite Volume Scheme," AIAA Paper 98-0231.

Kim, S.E., and Rhee, S.H. 2002 "Assessment of Eight Turbulence Models for a Three-Dimensional Boundary Layer involving Crossflow and Streamwise Vortices," AIAA 2002-0852, 40th AIAA Aerospace Sciences Meeting and Exhibit, Reno, NV, Jan.

Kotinis, M., Parsons, M. G., Lamb, T. and Sirviente, A. 2004 "Development and Investigation of the Ballast-Free Ship Concept," *Transactions* SNAME, **112**, pp. 206-240.

Kotinis, M. 2005 "Development and Investigation of the Ballast-Free Ship Concept," Ph.D. Dissertation, University of Michigan, Department of Naval Architecture and Marine Engineering.

Kotinis, M. and Parsons, M. G. 2007a "Numerical Investigation of the Flow at the Stern of a Ballast-Free Bulk Carrier Model" *Proceedings* of the 9th Int. Conference in Numerical Ship Hydrodynamics, Aug.

Kotinis, M. and Parsons, M. G. 2007b "Hydrodynamic Optimization of the Ballast-Free Ship Concept" *Transactions* SNAME, **115**, to be presented at the Annual Meeting Nov.

Mathur, S.R. and Murthy, J.Y. 1997 "A Pressure-Based Method for Unstructured Meshes," *Numerical Heat Transfer*, **31**, pp. 195-215.

Menter, F.R. 1994 Two-Equation Eddy-Viscosity Turbulence Models for Engineering Applications," *AIAA Journal*, **32**-8, pp.1598-1605, August.

Parsons, M. G. 2007 "Ballast-free ships: Investigations at the University of Michigan use local water for ballast," *Great Lakes Seaway Review*, **35**-2, pp.19 & 21, January-March.

Parsons, M. G. and Kotinis, M. 2006 "Seaway-Sized Bulk Carrier Model for Hydrodynamic Optimization of Ballast-Free Ship Design," GLMRI Annual Report, November 2006.

Rumelhart, D.E., Hinton, G.E., and Williams, R.J. 1986 "Learning internal representations by back-propagating errors," *Nature*, **323**, pp. 533-536

U. S. Patent #6,694,908 2004 "Ballast Free Ship System," U. S. Patent and Trademark Office, Washington, DC.

Van Lammeren, W. P. A., Van Manen, J. D. and Oosterveld, M. W. C. 1969 "The Wageningen B-Screw Series," *Transactions of SNAME*, **77**, pp. 269-317.